Multiscale Nature of Thixotropy and Rheological Hysteresis in Attractive Colloidal Suspensions under Shear

Multiscale Nature of Thixotropy and Rheological Hysteresis in Attractive Colloidal Suspensions under Shear

Safa Jamali,[1] Robert C. Armstrong,[2] and Gareth H. McKinley[2]
[1]Department of Mechanical and Industrial Engineering, Northeastern University, Boston, Massachusetts 02115 USA
[2]Department of Chemical Engineering, MIT Energy Initiative, Massachusetts Institute of Technology, Cambridge, Massachusetts 02139 USA
[3]Hatsopoulos Microfluids Lab, Department of Mechanical Engineering, Massachusetts Institute of Technology, Cambridge, MAMassachusetts 02139 USA

(Received 10 March 2019; published 10 December 2019)

Colloids with short range attractions self-assemble into sample-spanning structures, whose dynamic nature results in a thermokinematic memory of the deformation history, also referred to as "thixotropy." Here, we study the origins of the thixotropic effect in these time- and rate-dependent materials by investigating hysteresis across different length scales: from particle-level local measurements of coordination number (microscale), to the appearance of density and velocity fluctuations (mesoscale), and up to the shear stress response to an imposed deformation (macroscale). The characteristic time constants at each scale become progressively shorter, and hysteretic effects become more significant as we increase the strength of the interparticle attraction. There are also strong correlations between the thixotropic effects we observe at each scale.

DOI: 10.1103/PhysRevLett.123.248003

Attractive Brownian particles, even at small volume fractions, can form space-spanning networks that are viscoelastic in character and commonly referred to as gels [1–10]. These colloidal gels exhibit a wide range of complex physical or rheological behavior, owing to their microstructural evolution under applied stresses or deformations, including a strong rate- and time-dependent response to a specified deformation history which can be summarized concisely as a thixotropic elastoviscoplastic (TEVP) constitutive response [11,12]. Because of continuous formation and breakage of the interparticle bonds, secondary structures emerge under steady flow, which subsequently change the macroscopic response of the stress exerted by the fluid. The timescale for formation of these interparticle bonds competes with the timescale for bond breakage, which is primarily controlled by the applied shear, giving rise to a complex interplay between flow history and microstructure. This thixotropic effect, i.e., sensitivity not only to the rate of deformation, but also to its history, results in flow hysteresis [13].

Because of this structural hysteresis in thixotropic fluids, the stress response in the material at a given deformation rate and time may vary based on the preceding rates to which the fluid was exposed [14]. When the local shearing forces exerted on particle clusters due to the imposed flow are significantly larger than the attractive interparticle forces bringing the particles together, the particulate bonds are effectively broken, and colloidal gels thus asymptotically exhibit pseudo-Newtonian behavior with a constant shear viscosity at sufficiently high shear rates [15,16]. This enables such TEVP materials to be rejuvenated by an initial period of strong shearing. This is important with respect to repeatable experimental measurements on such materials, especially for depletion gels, as well as other soft glassy systems where the common initialization protocol is to submit the fluid to a very high deformation rate for long times to erase any existing memory [3,17].

A sequence of flow steps progressing from high to low shear rates, followed by a return to the initial high shear rate with a constant shearing time spent at each imposed rate results in well-defined and reproducible closed loops with measurable areas in the flow curve of such materials [14]. Divoux *et al.* showed that the areas enclosed by such hysteresis loops are strong functions of the time intervals over which the fluid is exposed to a given deformation rate [14]. Hysteresis areas measured from shear stress measurements and the inhomogeneous velocity profiles showed distinct bell-shaped distribution curves, each with a well-defined local maximum at a critical shearing time interval. Although similar in shape, the timescale defined by this local maximum was found to be larger for the velocity profiles compared to the timescale measured by the stresses. Recently, Radhakrishnan *et al.* [18] showed that a phenomenological fluidity model can reproduce such hysteresis loops. These experimental measurements and numerical simulations of the flow hysteresis phenomenon in thixotropic fluids clearly indicate that there is a material-dependent characteristic timescale; however, observation of these thixotropic dynamics has largely been limited to macroscopic measurables of a system, namely, the stress

and the local velocity gradient, and such measures do not provide a robust connection to the underlying microstructural evolution, or the possible development of shear localization events such as transient shear banding in time-dependent materials. Here we provide a detailed view of thixotropy across length scales, and systematically investigate a wide range of attraction strengths between the particles. We provide measures of flow hysteresis at three different length scales and based on three different measures: (i) the average number of particle-particle bonds, i.e., the coordination number $\langle Z \rangle$ as a local and *microscopic* measure, (ii) number density fluctuations in the fluid, as a measure of *mesoscopic* structures at the particulate cluster level, and (iii) the average shear stress exerted by the sheared suspensions of attractive particles as a *macroscopic* or bulk measure of the system. For comparative purposes, we also compute the local kinematic measure of hysteresis described in Ref. [14].

Prior studies have shown that the flow behavior of attractive colloidal gels can be understood in terms of the ratio of shear forces to the strength of attraction between the particles [15,16,19]. This ratio is commonly referred to as the Mason number, $\mathrm{Mn} = 6\pi\eta\dot{\gamma}a^3/\Gamma$ where η is the suspending fluid viscosity, a is the radius of a particle, $\dot{\gamma}$ is the imposed deformation rate, and Γ is the strength of attraction between particles. At $\mathrm{Mn} < 10^{-2}$ shear forces are not strong enough to break the particulate network and thus shear compaction is observed [15,16]. At intermediate flow rates, $10^{-2} < \mathrm{Mn} < 10^{0}$ constant break up and reformation of particulate bonds results in mesoscopic heterogeneities and a strong time-dependent stress response to the applied deformation [20,21]. At large flow rates, $\mathrm{Mn} > 10^{0}$ the strong shear forces can effectively break the network into individual particles, and thus a pseudo-Newtonian behavior is observed. The dimensionless group, Mn, defined here also has been reported previously, and referred to as the Peclet number of depletion, by Koumakis *et al.* [22], where authors showed the dependence of an average coordination number on the attraction strength between the short-range attractive particulate gels under different shear rates. To observe the flow hysteresis in our computational flow protocol the colloidal gels are submitted first to a decreasing shear rate flow, from a high initial Mn above unity (where a particulate network is absent), down to the lowest shear rates accessible (over three decades in applied shear rates) before then being exposed again to progressively higher shear rates.

A modified dissipative particle dynamics (DPD) scheme is employed in this work [15,16,23–25] as a computational platform that enables study of the evolution of large particulate systems over long timescales. In this Letter, we fix the volume fraction of particles at $\phi = 0.15$ corresponding to 10^4 colloidal, and 7.12×10^5 solvent particles, respectively. The range of interaction was kept at $\kappa^{-1} = 0.2a$, and the strength of attraction was varied between $0 \leq \Gamma \leq 50k_BT$. Time is scaled with the diffusive time of a single bare particle $\tau = a^2/D$, where D is the diffusion coefficient of a single particle, $\tau = 1.42r_c(m/k_BT)^{1/2}$. All simulations were initiated by using a random distribution of particles with size polydispersity of 5%, and an initial velocity profile corresponding to $\dot{\gamma} = 5$. We then ramp the shear rate down to $\dot{\gamma} = 10^{-3}$ in 16 logarithmacally spaced steps of length Δt, with $1 \leq \Delta t/\tau \leq 100$. The corresponding Mason number and the DPD shear rate are linearly related, such that $\mathrm{Mn} = 6\pi\eta\dot{\gamma}a^3/\Gamma$ (and so $\mathrm{Mn} = 1.28\dot{\gamma}$ for $\Gamma = 50k_BT$, and $\mathrm{Mn} = 64.1\dot{\gamma}$ for $\Gamma = 1k_BT$). Our shearing protocol and our range of attraction strengths simulated thus span 5 orders of magnitude in Mn, $10^{-3} \leq \mathrm{Mn} \leq 3.2 \times 10^2$.

To compactly represent our results we use the ensemble-averaged coordination number $\langle Z \rangle$ to provide a local measure of microstructure. As a mesoscale measure we use the average number density fluctuation (NDF), to quantify the local differences in the number density of particles, $\langle N \rangle$, throughout the sample: $\mathrm{NDF} = (\langle N^2 \rangle - \langle N \rangle^2)/\langle N \rangle$ [21,26]. In Fig. 1 we show typical snapshots of the structures formed at maximum, minimum, and intermediate imposed shear rates. Figure 1(a) provides a graphical representation of the applied flow protocol for an attractive colloidal system with $\phi = 0.15$ and attraction strength of $10k_BT$ (red and blue stepped curves). There is a sequence of shear rate steps taken during ramp down or up (with $\Delta t = 10\tau$), accompanied by the stress, average coordination number, and number density fluctuations. Figures 1(c)–1(e) show the same three measures plotted against the Mason number. Figure 1(b) shows kymographs of the instantaneous velocity profiles across the velocity gradient direction at the same times as Fig. 1(a). The results in Figs. 1(c)–1(e) clearly show a hysteretic response for all three measurables. As the system undergoes gelation or flocculation during the ramp-down process, particle bonds are formed and thus the average coordination number increases monotonically with decreasing Mn. Conversely, there is a progressive breakdown of the microstructure when subject to an increasing shear rate protocol. This coincides with an even clearer hysteresis loop in the number density fluctuations; however, the monotonic increase of the mesoscale heterogeneities during the ramp-down protocol is followed by a further shear-induced increase during the initial ramp-up in Mn. This illustrates that at the same shear rate not only are the heterogeneities dissimilar, but also that the critical shear rate or stress for fluidization strictly depends on the kinematic memory of the material [27–29]. The DPD results in Figs. 1(c)–1(d) show that upon increasing the deformation rate, the particle network initially breaks into large clusters in which the average number of particle bonds can be large, compared to the initial gradual formation and progressive growth of the particle network when subjected to a decreasing shear profile. Although morphological snapshots as well as the number density fluctuations show clear differences

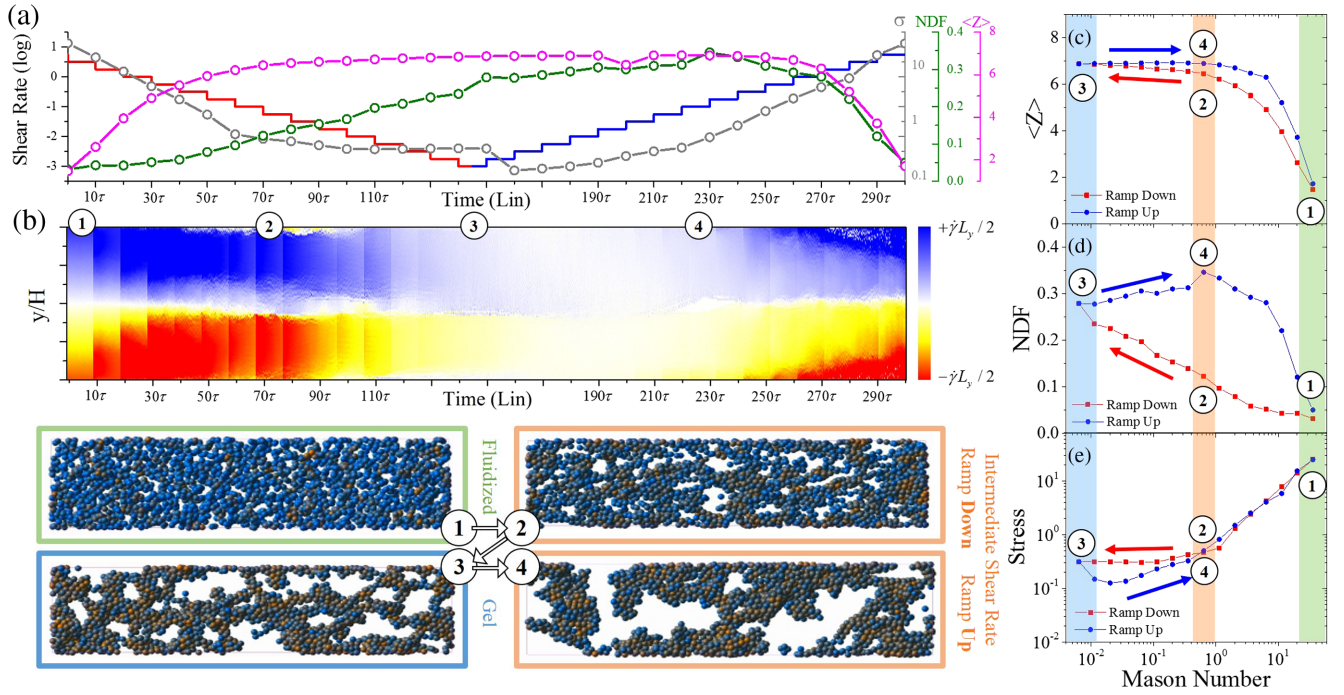

FIG. 1. (a) The imposed shear protocol, with logarithmic sampling of shear rates against time, accompanied with measured $\langle Z \rangle$, NDF, and shear stress σ, for a system of attractive colloids with $\phi = 0.15$ and $\Gamma = 10 k_B T$ and waiting time of $\Delta t = 10\tau$ at each DPD shear rate. (b) Kymograph of the velocity profile across the velocity gradient direction, as a function of time. Snapshots of the particles at the maximum (green, 1), minimum (blue, 3) and intermediate shear rates (in orange, 2 and 4) show typical structures of the particulate system, also marked in the hysteresis curves. (c)–(e) Flow hysteresis loops are shown for average coordination number, number density fluctuation, and shear stress against applied Mn, respectively.

between points indicated as 3 and 4 in Fig. 1, the coordination number is rather similar; however, the distribution of coordination numbers can vary significantly between the two structures [15,16]. These structural evolutions also change the macroscopic mechanical response of the material [Fig. 1(e)], where formation of these clusters gives rise to a finite yield stress and dynamic yielding of the material [30,31]. Moreover, careful comparison of the kymograph presented in Fig. 1(b) with the corresponding shear rates or stresses presented in Fig. 1(a) shows that two similar velocity profiles may result in different shear stresses, and different velocity profiles may result in similar shear stresses (for individual scaled velocity profiles, $v_x(y,t)/\dot{\gamma} L_y$, during each shear step, see the Supplemental Material [32]). Although the local velocity profiles clearly indicate the presence of flow heterogeneities such as shear banding, they do not necessarily correlate directly with the measured shear stresses. Similar conclusions were reached experimentally by Ref. [14].

Using the three hysteresis measures presented in Figs. 1(c)–1(e), one can define quantitative metrics for material thixotropy, based on the following equations for the micro-, meso-, and macroscales, respectively:

$$A_Z \equiv \int_{\dot{\gamma}_{\min}}^{\dot{\gamma}_{\max}} |\Delta \langle Z(\dot{\gamma}) \rangle| d(\log \dot{\gamma}), \tag{1}$$

$$A_{\mathrm{NDF}} \equiv \int_{\dot{\gamma}_{\min}}^{\dot{\gamma}_{\max}} |\Delta \mathrm{NDF}(\dot{\gamma})| d(\log \dot{\gamma}), \tag{2}$$

$$A_\sigma \equiv \int_{\dot{\gamma}_{\min}}^{\dot{\gamma}_{\max}} |\Delta \sigma(\dot{\gamma})| d(\log \dot{\gamma}). \tag{3}$$

Following Ref. [14] we also compute the characteristic thixotropic timescale that can be measured from differences in the velocity profiles at the end of each applied shear rate using

$$A_v \equiv \int_{\dot{\gamma}_{\min}}^{\dot{\gamma}_{\max}} \int_{-L/2}^{L/2} |\Delta v(\dot{\gamma}, y)| d(\log \dot{\gamma}), \tag{4}$$

where $\Delta v(\dot{\gamma}, y) = v_{\mathrm{up}}(\dot{\gamma}, y) - v_{\mathrm{down}}(\dot{\gamma}, y)$ is the difference in the fluid velocity in the flow direction (x), at a given position in the velocity gradient direction (y), in the ramp-up and ramp-down shearing protocols.

In Fig. 2(a) we present the evolution in the computed stress hysteresis as a function of the time interval Δt, over which each shear rate is imposed, for a wide range of different interparticle attraction strengths. It should be noted that each point in Fig. 2 represents the integrated hysteresis areas measured in our down or up flow protocol, similar to those presented in Figs. 1(c)–1(e). The general trends observed in Fig. 2(a) are consistent with those

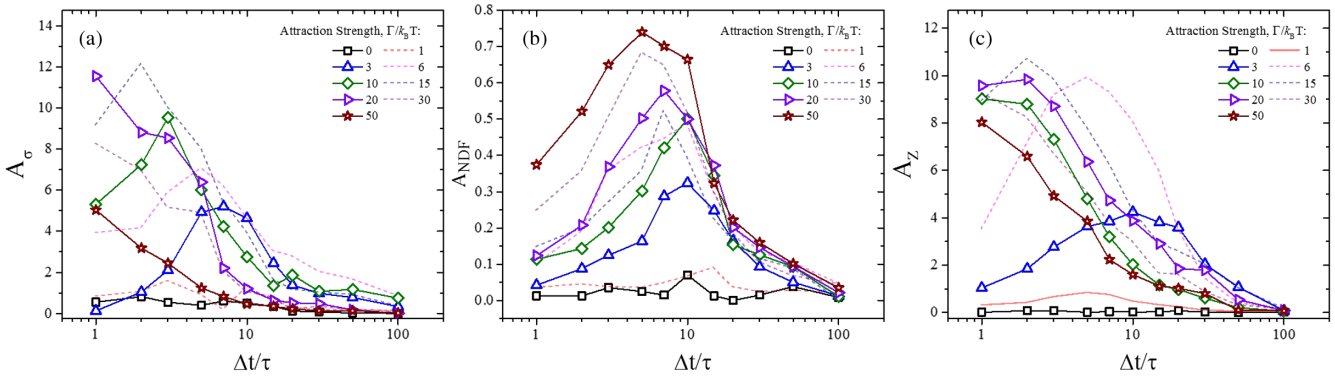

FIG. 2. Hysteresis measures for an attractive suspension with $\phi = 0.15$ calculated based on (a) the shear stress, (b) the number density fluctuations, and (c) the average coordination number as a function of the shearing time at each shear rate Δt for a range of different attraction strengths between the particles. Some data are presented using dashed lines for clarity.

reported by Divoux *et al.* [14] for laponite and carbon black gels, exhibiting a local maximum for a specific shearing time Δt^*. Moreover, the results in Fig. 2(a) suggest two major consequences of increasing Γ. First, the characteristic timescale at which the maximum hysteresis occurs decreases progressively to shorter times with increasing interparticle attraction strength. This continues to the point where (for very strong attractions, $\Gamma > 15k_BT$) the local maximum would correspond to very short shearing times ($\Delta t/\tau < 1$), not captured by the shearing protocol and hence only the decreasing tail of the distribution for $\Delta t > \Delta t^*$ is observed. Second, the maximum hysteresis area increases by increasing the attractive interparticle interactions. Particles with stronger attractions not only form bonds, clusters, and sample-spanning networks faster than weakly bonding particles, but also show a larger sensitivity to the history of flow. The control simulations with minimal attractive interactions show no significant hysteresis, as expected for hard-sphere suspensions at moderate volume fractions. Figure 2(b) shows the hysteresis on mesoscopic scales, A_{NDF}, as a function of the time interval. Although this measure shows a monotonic increase as we strengthen the attraction between the particles, the characteristic timescale shows a rather weak dependence on the strength of the attractive forces. This suggests that regardless of the attraction between individual particles, the clusters of particles form and break at similar timescales controlled by the balance between diffusion and the imposed rate of shearing.

Local hysteresis variations are presented in Fig. 2(c), based on measurements of the average coordination number. These results are in close agreement with the results in Fig. 2(a), suggesting that the macroscopic hysteresis measures of this thixotropic system closely track the microscopic changes of the material. Bulk thixotropic effects, namely, the time- and history-dependent stress response, thus originate from local microscopic effects, rather than from heterogeneities in the system. For example, particles that are strongly attractive ($\Gamma \geq 20k_BT$) exhibit very short timescales for formation of local particle-particle bonds, which in turn significantly changes the hysteretic stress response of the material, while the characteristic timescales for clusters of particles to show sensitivity to the flow history and transiently develop shear bands are much longer within the same thixotropic material. Although the mesostructures in the system do not vary significantly [for short shearing times $\Delta t < \Delta t^*$] for strongly associating particles, the change in microstructure leads to a significant difference in the macroscopic stress response of the thixotropic material. This is of particular utility to experimental rheologists who seek to make rapid measurements of the rheological flow curve in a shearing material without worry about the development of kinematic inhomogeneities such as shear bands or wall slip.

One can measure the characteristic timescale associated with the largest hysteresis behavior of a material at any given scale by fitting a log-normal distribution of the form $A_{(i)} = A^*_{(i)} \exp\{-[\log(\Delta t/\tau^{(i)}_{\mathrm{thix}})/w_{(i)}]^2\}$ to the curves in Fig. 2, where the characteristic thixotropic timescale [$\tau^{(i)}_{\mathrm{thix}}$ with $(i) = \sigma$, NDF, $\langle Z \rangle$, v respectively] for each process is found from the local maximum in each hysteresis measure. The timescales associated with structural evolution across the different scales are presented in Fig. 3(a) as a function of attraction strength, Γ. The data in Fig. 3(a) show that mesoscale structures are the least sensitive to individual particle interactions, while the microstructural and macroscopic measures show a significant dependence on the strength of the interaction potential. There is a clear and surprising separation of the characteristic timescales for each dynamical process described by the hysteresis metrics in Eqs. (1)–(4). First, this analysis shows that the timescale for particle-level hysteresis closely tracks the thixotropy measured by the shear stresses. It is also evident that the thixotropic timescale measured from the inhomogeneous velocity profiles are in close agreement with the ones measured from NDF. This suggests that although mesoscale structural hysteresis is strongly connected to flow heterogeneities such as shear banding, the rheological

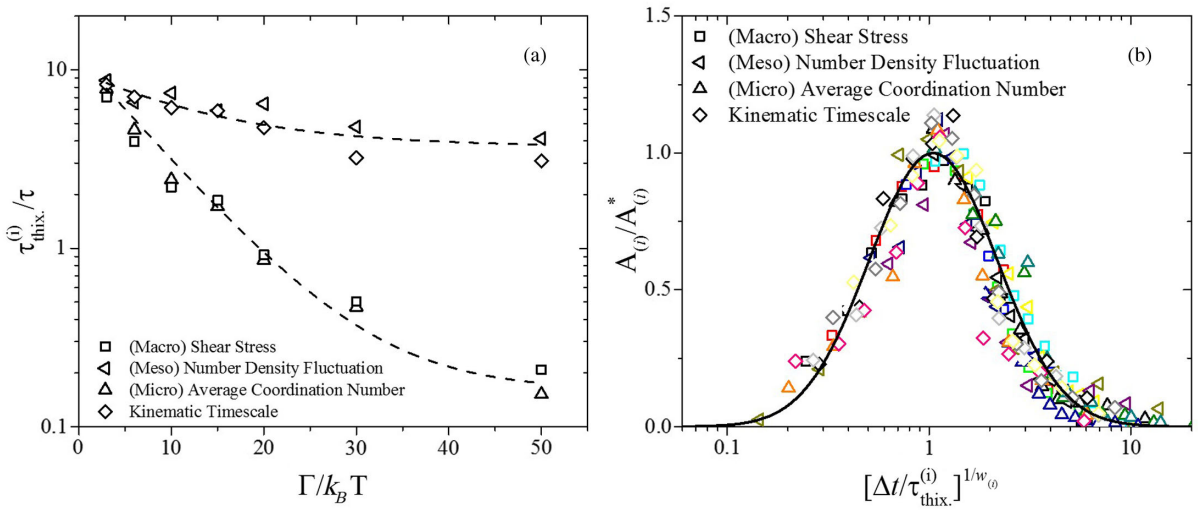

FIG. 3. (a) Characteristic thixotropic time, $\tau^{(i)}_{\mathrm{thix}}$, where i denotes each of the different measures defined in Eqs. (1)–(4), scaled by the diffusive time of a single particle as a function of attraction strength between particles, and (b) the normalized hysteresis area, A/A^*, for all fluids simulated vs normalized waiting time $[\Delta t/\tau_{\mathrm{thix}}]^{1/w}$, where A^*, and w are the parameters of the log-normal fits (solid line).

hysteresis measured through shear stress loops is more closely related to the local changes in the particulate system rather than the mesostructures.

Using the parameters of the log-normal distribution fits, $A^*_{(i)}$ and $w_{(i)}$, we can collapse the entirety of our results presented in Fig. 2, as shown in Fig. 3(b). This clearly shows that at each scale at which the fluid is interrogated a unique thixotropic timescale can be identified and measured, for each attraction strength.

The rheological response of attractive colloidal systems shows strong sensitivity not only to the rate of an imposed deformation, but also to its history. This strong thixotropic effect can be observed across different length scales or timescales, from the particle-level microstructure, to cluster-level kinematic heterogeneities, and up to macroscopic shear stress resulting from a deformation rate history. The hysteresis is much more pronounced when the attraction strength is increased, showing that transport of strongly attractive particles is much more sensitive to the flow history, than it is for weakly attractive particles. We determined a characteristic hysteresis time for these thixotropic loops based on the hysteresis areas calculated at each scale. At the largest and the smallest scales the thixotropic timescales $\tau^{\sigma}_{\mathrm{thix}}$ and $\tau^{\langle z\rangle}_{\mathrm{thix}}$ agree closely and are strong functions of the attraction strength, Γ/k_BT. The timescales associated with local cluster formation and with the appearance of shear bands are also strongly correlated, but are only weakly dependent on material properties.

For weak attractions, $\Gamma < 10k_BT$, these two different processes shown in Fig. 3(a) happen on roughly equivalent timescales; i.e., rheological hysteresis and shear localization cannot easily be separated, and therefore slowly varying flow protocols with $\Delta t \gg \tau^{i}_{\mathrm{thix}}$ are required to minimize the hysteretic effects. Contrarily, for strong attractions, $\Gamma \geq 10k_BT$, the separation of timescales is large and thus both slow and fast flow loops will result in measurement of true material properties under essentially homogenous flow conditions. A slow loop with $\Delta t \gg \tau^{(\sigma)}_{\mathrm{thix}}$ leads to a quasiequilibrium flow curve, whereas a very fast thixotropic ramp down with $\Delta t \ll \tau^{(v)}_{\mathrm{thix}}$ leads to a "quenched" state with a very different microstructure and a different flow curve. We show a computational comparison of such trajectories at $\Gamma = 20k_BT$ in the Supplemental Material [32]. Similar quenched states have been demonstrated experimentally in strongly attractive carbon black gels [33,34]. Our findings suggest that by controlling (i) the history of applied deformations under which aggregation occurs, and (ii) understanding the available time for particle clusters to lose their memory of structuration processes at each scale, we can control and engineer different microstructures and different rheological states in colloidal gels and other soft glassy systems. Considering analogies to the anisotropic microstructural evolutions, and continuous formation and breakup of particle cages observed in hard-sphere colloidal glasses [35], a similar thixotropic and hysteresis behavior can be studied for dense colloidal systems.

[1] P. J. Lu, E. Zaccarelli, F. Ciulla, A. B. Schofield, F. Sciortino, and D. A. Weitz, Gelation of particles with short-range attraction, Nature (London) **453**, 499 (2008).
[2] C. J. Rueb and C. F. Zukoski, Viscoelastic properties of colloidal gels, J. Rheol. **41**, 197 (1997).
[3] E. Zaccarelli, Colloidal gels: Equilibrium and non-equilibrium routes, J. Phys. Condens. Matter **19**, 323101 (2007).

[4] E. Zaccarelli and W. C. K. Poon, Colloidal glasses and gels: The interplay of bonding and caging, Proc. Natl. Acad. Sci. U.S.A. **106**, 15203 (2009).
[5] J. Bergenholtz, W. C. K. Poon, and M. Fuchs, Gelation in model colloid-polymer mixtures, Langmuir **19**, 4493 (2003).
[6] W. C. K. Poon, The physics of a model colloid-polymer mixture, J. Phys. Condens. Matter **14**, R859 (2002).
[7] F. W. Starr, J. F. Douglas, and S. C. Glotzer, Origin of particle clustering in a simulated polymer nanocomposite and its impact on rheology, J. Chem. Phys. **119**, 1777 (2003).
[8] J. M. Kim, J. Fang, A. P. R. Eberle, R. Castañeda-Priego, and N. J. Wagner, Gel Transition in Adhesive Hard-Sphere Colloidal Dispersions: The Role of Gravitational Effects, Phys. Rev. Lett. **110**, 208302 (2013).
[9] S. W. Sides, B. J. Kim, E. J. Kramer, and G. H. Fredrickson, Hybrid Particle-Field Simulations of Polymer Nanocomposites, Phys. Rev. Lett. **96**, 250601 (2006).
[10] H. Verduin and J. K. G. Dhont, Phase diagram of a model adhesive hard-sphere dispersion, J. Colloid Interface Sci. **172**, 425 (1995).
[11] J. Mewis and N. J. Wagner, Thixotropy, Adv. Colloid Interface Sci. **147–148**, 214 (2009).
[12] R. G. Larson, Constitutive equations for thixotropic fluids, J. Rheol. **59**, 595 (2015).
[13] M. Geri, R. Venkatesan, K. Sambath, and G. H. McKinley, Thermokinematic memory and the thixotropic elastoviscoplasticity of waxy crude oils, J. Rheol. **61**, 427 (2017).
[14] T. Divoux, V. Grenard, and S. Manneville, Rheological Hysteresis in Soft Glassy Materials, Phys. Rev. Lett. **110**, 018304 (2013).
[15] A. Boromand, S. Jamali, and J. M. Maia, Structural fingerprints of yielding mechanisms in attractive colloidal gels, Soft Matter **13**, 458 (2017).
[16] S. Jamali, G. H. McKinley, and R. C. Armstrong, Microstructural Rearrangements and their Rheological Implications in a Model Thixotropic Elastoviscoplastic Fluid, Phys. Rev. Lett. **118**, 048003 (2017).
[17] P. J. Lu and D. A. Weitz, Colloidal particles: Crystals, glasses, and gels, Annu. Rev. Condens. Matter Phys. **4**, 217 (2013).
[18] R. Radhakrishnan, T. Divoux, S. Manneville, and S. M. Fielding, Understanding rheological hysteresis in soft glassy materials, Soft Matter **13**, 1834 (2017).
[19] J. D. Park and K. H. Ahn, Structural evolution of colloidal gels at intermediate volume fraction under start-up of shear flow, Soft Matter **9**, 11650 (2013).
[20] J. M. Kim, A. P. R. Eberle, A. K. Gurnon, L. Porcar, and N. J. Wagner, The microstructure and rheology of a model, thixotropic nanoparticle gel under steady shear and large amplitude oscillatory shear (LAOS), J. Rheol. **58**, 1301 (2014).
[21] B. Rajaram and A. Mohraz, Microstructural response of dilute colloidal gels to nonlinear shear deformation, Soft Matter **6**, 2246 (2010).
[22] N. Koumakis, E. Moghimi, R. Besseling, W. C. K. Poon, J. F. Brady, and G. Petekidis, Tuning colloidal gels by shear, Soft Matter **11**, 4640 (2015).
[23] S. Jamali, A. Boromand, N. Wagner, and J. Maia, Microstructure and rheology of soft to rigid shear-thickening colloidal suspensions, J. Rheol. **59**, 1377 (2015).
[24] S. Jamali, M. Yamanoi, and J. Maia, Bridging the gap between microstructure and macroscopic behavior of monodisperse and bimodal colloidal suspensions, Soft Matter **9**, 1506 (2013).
[25] M. Whittle and K. P. Travis, Dynamic simulations of colloids by core-modified dissipative particle dynamics, J. Chem. Phys. **132**, 124906 (2010).
[26] A. Mohraz and M. J. Solomon, Orientation and rupture of fractal colloidal gels during start-up of steady shear flow, J. Rheol. **49**, 657 (2005).
[27] T. Divoux, C. Barentin, and S. Manneville, From stress-induced fluidization processes to Herschel-Bulkley behaviour in simple yield stress fluids, Soft Matter **7**, 8409 (2011).
[28] T. Divoux, D. Tamarii, C. Barentin, S. Teitel, and S. Manneville, Yielding dynamics of a Herschel-Bulkley fluid: A critical-like fluidization behaviour, Soft Matter **8**, 4151 (2012).
[29] V. Grenard, T. Divoux, N. Taberlet, and S. Manneville, Timescales in creep and yielding of attractive gels, Soft Matter **10**, 1555 (2014).
[30] C. J. Dimitriou and G. H. McKinley, A comprehensive constitutive law for waxy crude oil: A thixotropic yield stress fluid, Soft Matter **10**, 6619 (2014).
[31] A. Vázquez-Quesada and M. Ellero, SPH modeling and simulation of spherical particles interacting in a viscoelastic matrix, Phys. Fluids **29**, 121609 (2017).
[32] See Supplemental Material at http://link.aps.org/supplemental/10.1103/PhysRevLett.123.248003 for individual velocity profiles during the shearing ramps, an example of quenched vs quasi-equillibrium flow protocols and alternate functional forms to the log-normal fit shown in Fig. 3(b).
[33] A. Helal, T. Divoux, and G. H. McKinley, Simultaneous Rheoelectric Measurements of Strongly Conductive Complex Fluids, Phys. Rev. Applied **6**, 064004 (2016).
[34] V. Grenard, N. Taberlet, and S. Manneville, Shear-induced structuration of confined carbon black gels: Steady-state features of vorticity-aligned flocs, Soft Matter **7**, 3920 (2011).
[35] N. Koumakis, M. Laurati, S. U. Egelhaaf, J. F. Brady, and G. Petekidis, Yielding of Hard-Sphere Glasses during Start-Up Shear, Phys. Rev. Lett. **108**, 098303 (2012).